3D Finite Element Analysis for Arcing Chamber Optimization of the Current-limiting Circuit Breaker

ELENA OTILIA VIRJOGHE[*]
DIANA ENESCU[**]
MARCEL IONEL[**]
FLORIN MIHAIL STAN[*]
Department of Control Engineering, Informatics and Electrical Engineering[*]
Department of Electronic, Telecommunication and Power Engineering[**]
"VALAHIA" University of Targoviste
Unirii Ave.no.18-20
ROMANIA
otiliavirjoghe@yahoo.com, denescu@valahia.ro, ionel.marcell@yahoo.com
flo_stan@gmail.com

Abstract: - Direct current, which was one of the main means of distributing electric power, is still widespread today in the electrical plants supplying particular industrial applications. The advantages in terms of settings, offered by the applicants of d.c. motors and by supply through a single line, make direct current supply a good solution for railway and underground systems, trams, lifts and other transport means.
The paper presents the calculation of the magnetic field in the arcing chamber of the current-limiting circuit breaker of the direct current 1250 A, 750 V. Current-limiting circuit breakers play an important role in electrical low-voltage circuits. Due to the high short-circuit currents it is necessary a very short time to switch off the defective branch. For this the current limiting circuit breakers are conceived as elaborated solutions especially for the arc quenching system, meaning the path of current and the arcing chamber. In this paper the authors present few optimization solutions of some quenching systems which will lead to more performing constructive choices. The finite element software package ANSYS is use for calculation of the magnetic field components.

Key-Words: - arcing chamber, magnetic field, current-limiting circuit breaker, finite element method, software package ANSYS, optimization, numerical simulation

1 Introduction

Computer-aided analysis of field distribution for evaluating electromagnetic device or component performance has become the most advantageous way of design. Analytical methods have limited uses and experimental methods are time requirement and expensive [1].
The particular torque-speed characteristic curve and the ease with which the speed itself can be regulated have led to the use of d.c. motors in the field of electric traction. Direct current supply gives also the great advantage of having the contact line consisting of a single conductor since the rails provide the return conductor [2]. Direct current is used above all in urban transport that is trolleybuses, trams and underground railways with a supply voltage of 600V or 750V, up to 1000V. The use of direct current is not limited to vehicle traction only, but direct current represents a supply source for the auxiliary circuits on board vehicles. In such cases accumulator batteries are installed, which constitute an auxiliary power supply source to be used if the external one should fail.
It is very important that this power supply is guaranteed since the auxiliary circuits may supply essential services, such as: air conditioning plants, internal and external lighting circuits, emergency brake systems, electrical heating systems, etc.. The applications of circuit-breakers in d.c. circuits for electric traction in general can be summarized as follows:
-protection and operation of both overhead and rail contact lines;
-protection of air compressors on board underground and train cars;
-protection of distribution plants for services and signaling systems;
-protection of d.c. supply sources (accumulator batteries);
-protection and operation of d.c. motors [2].

The software package ANSYS can be used for investigation of the magnetic field distribution (the magnetic flux density, the magnetic field strength and the magnetic vector potential) and basic electromagnetic characteristics (inductance and electromagnetic force) of the arcing chamber of the current-limiting circuit breaker of the direct current 1250 A, 750 V. A typical magnetic field problem is described by defining the geometry, material properties, currents, boundary conditions, and the field system equations. The computer requires the input dates, the numerical solution of the field equation and output of desired parameters. If the values are found unsatisfactory, the design modified and parameters are recalculated. The process is repeated until optimum values for the design parameters are obtained.
This program is based on the finite element method for solving Maxwell equations and can be used for electromagnetic field modeling where the field is electrostatics, magnetostatics, eddy currents, time-invariant or time-harmonic and permanent magnets [3].
The Finite Elements method assures sufficient accuracy of electromagnetic field computation and very well flexibility when geometry is modeled and field sources are loaded [1].
3D characterization of electrical arc in circuit breakers is made possible today from various types of computational codes and applications [8]-[10].

2 Arcing chamber of the current – limiting circuit breaker

This current – limiting circuit breaker is used in urban transport that is trolleybuses, trams and underground railways. The supply voltage for urban transport is 600 V or 750 V up to 1000 V.
Arcing chamber of the current – limiting circuit breaker uses for the electric arc extension through electrode effect for arc quenching, the magnetic blow-out system (realized with ferromagnetic plates) [4].
The most significant advancement was the development of the arc chamber, which is a boxlike component device that contains a number of either metallic or insulated plates. Additionally, in most of the designs, when intended for medium voltage applications, the arc chamber includes a magnetic blow-out coil [5].
In a current – limiting circuit breaker, increasing the resistance of the arc in effect increases the arc voltage. Thus, to effectively increase the arc voltage any of the following means can be used:

1. Increase the length of the arc, which increases the voltage drop across the positive column of the arc.
2. Split the arc into a number of shorter arcs connected in series. What this does is that instead of having a single cathode and anode at the ends of the single arc column there are now a multiplicity of cathode and anode regions, which have additive voltage drops. Although the short arcs reduce the voltage of each individual positive column, the summation of all the voltage drops is usually greater than that of a single column; furthermore, if the number of arcs is large enough so that the summation of these voltage drops is greater than the system voltage a quick extinction of the arc is possible.
3. Constricting the arc by constraining it between very narrow channels. This in effect reduces the cross-section of the arc column and thus increases the arc voltage.

With both of the last two suggested methods there is an added benefit, which is the additional cooling of the arc as the result of the high energy storage capacity provided by the arc chute plates that are housed inside of the arc chamber itself [5].

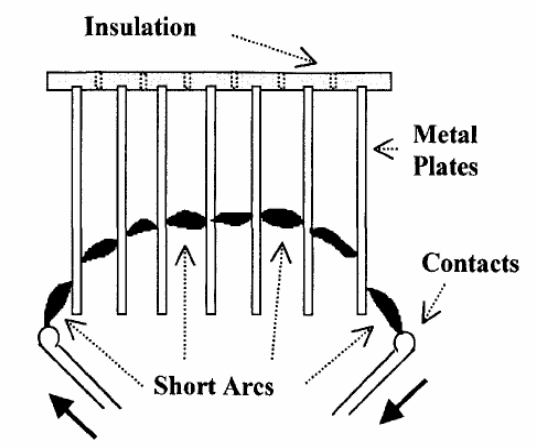

Fig.1 Outline of a plain arc chamber used in low voltage circuit breakers [5]

An arc chamber can be described as a box shaped structure made of insulating materials. A schematic representation of this type of arc chamber, which is used almost exclusively in low voltage applications, is shown in Fig.1.
Each arc chamber surrounds a single pole of the circuit breaker independently, and it provides structural support for a set of arc plates and in some cases, when so equipped, it houses a built-in magnetic blow-out coil [5].
Basically there are two types of arc chambers, where each type is characterized primarily by the material of the arc plates that are used. Some arc

plates are made of soft steel and in some cases are nickel plated. In this type of arc chamber the arc is initially guided inside the plates by means of arc runners, which is simply a pair of modified arc horns. Subsequently the arc moves deeper into the arc chamber due to the forces produced by the current loop and the pressure of the heated gases [5]. In order to increase and to control the motion of the arc, vertical slots are cut into the plates. The geometrical pattern of these slots varies among circuit breaker manufacturers, and although there may be some similarities in the plate designs, each manufacturer generally has a unique design of its own. When the arc comes in contact with the metal plates it divides into a number of shorter arcs that bum across a set of adjacent plates. The voltage drop that is observed across each of these short arcs is usually about 30 to 40 volts, the majority of this voltage being due to the cathode and anode drop of each arc. The voltage drop of the positive column depends on the plate spacing, which in turn determines the length of the arc's positive column [5].

2.1 The physical model of the arcing chamber

In Fig.2 is presented the construction plan of the current path which includes the output terminals A, B, the conducting bars 1,2, the brake contacts 3 (lasting contacts) and 4 (arc brake contacts), the slopes 5, 6 placed in the arcing chamber CS. Within the arcing chamber there are the ferromagnetic plates 7, the insulated plates 8 and in the outside of it there are the ferromagnetic shapes 9.

The slopes have a smooth surface and they are made of copper because this material gives a good mobility and a high thermal conductivity. The ferromagnetic shapes 9 intensify the magnetic field and direct it to the arcing chamber so that a stronger ascending force acting on the electric arc base (along the slopes) and also on the electric arc, inside of the arcing chamber, is obtained [7].

The accessional circulation of heating air and the intensification of the magnetic field (produced by ferromagnetic plates 7) bring the arc extinction by direct acting on the arc core and by restrained displacement of the arc base. Thus, the electric arc is moving through the arcing chamber. The force acting on the arc core, placed into the magnetic field (generated by the electric current which follows to be broken), is proportional to the current strength, the magnetic field strength and the length of the arc column [3].

Physical model partially reproduces conditions inside of the current-limiting circuit breaker's arcing chamber [4]. This model represents the current path, made of copper, dimensions of 10x15 mm^2, with parallelepiped shape. The current path is crossed by a $8.33 \cdot 10^6$ A/m^2 density current. The two plates made of a ferromagnetic material, have a shape of trapezoidal prism, with 190 mm small end length, 250 mm length of the large end, 60 mm in height and 3 mm thickness. Electric arc slopes are made of copper, 30 mm width and 6 mm thickness.

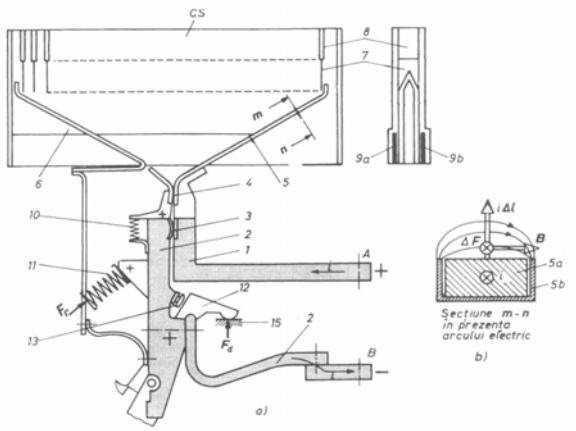

Fig.2 The sketch of the current – limiting circuit breaker [4]

2.2 Analysis of three-dimensional electromagnetic problems by FEM

Due to the physical model asymmetry, the three-dimensional modeling of magnetostatic field was necessary. In a three-dimensional case it is described by elliptic equation Laplace-Poisson.

Magnetic energy functional of magnetostatic field has a following expression [6]:

$$\Im(\overline{A}) = \int_D \left\{ \left(\int_0^{\overline{B}} \overline{H} d\overline{B} \right) - \overline{J}\overline{A} + \frac{\nu}{2} (\mathrm{div}\overline{A})^2 \right\} dD + \int_\Sigma (\overline{H} \cdot \overline{A}) \cdot \overline{n}_\Sigma d\Sigma - \int_s \overline{J}_s \overline{A} dS \quad (1)$$

The first two terms of integral on computing field 3D in (1) are directly obtained by means of general functional in conditions of steady state magnetic field, that means:

$$\partial / \partial t = 0 , \ \overline{E} = \overline{D} = 0 \ \text{ and } \rho_v = 0 . \quad (2)$$

The last term includes the condition on an eventual discontinuity surface S form the computing field on it is given the layer density of conduction current $\overline{J}_s$.

The passing condition is [6]:

$$\begin{aligned}&\mathrm{rot}_s\,\bar{H}=\bar{n}_s x\left[\bar{H}\right]_s=\bar{J}_s \text{ and}\\&\mathrm{div}_s\,\bar{B}=\bar{n}_s\cdot\left[\bar{B}\right]=0\,.\end{aligned}\tag{3}$$

Equaling with zero of the first variation of functional imposes:

$$\begin{aligned}&\delta F\left(\delta\bar{A}\right)=\int_D\left(\bar{H}\mathrm{rot}\delta\bar{A}-\bar{J}\delta\bar{A}+\nu\,\mathrm{div}\bar{A}\cdot\mathrm{div}\delta\bar{A}\right)dD+\\&+\int_\Sigma\left(\bar{H}\times\delta\bar{A}\right)\cdot\bar{n}_E d\Sigma-\int\bar{J}_S\delta\bar{A}\,dS=\\&\int_D\left\{\left(\mathrm{rot}\bar{H}-\bar{J}-\mathrm{grad}\left(\nu\,\mathrm{div}\bar{A}\right)\right)\delta\bar{A}\right\}dD+\\&+\int_\Sigma\left\{\left(\bar{H}\times\delta\bar{A}\right)+\left(\delta\bar{A}\times\bar{H}\right)+\delta\bar{A}\cdot\nu\,\mathrm{div}\bar{A}\right\}\bar{n}_\Sigma d\Sigma\\&+\int_S\left\{\left(\left(\bar{n}_\Sigma\times\left[\bar{H}\right]_\Sigma\right)-\bar{J}_S\right)\delta\bar{A}\right\}dS=0\end{aligned}\tag{4}$$

where the following definition $\bar{B}=\mathrm{rot}\bar{A}$, the identity vectorial [6]:

$$\bar{H}\mathrm{rot}\delta\bar{A}=\mathrm{div}\left(\delta\bar{A}\times\bar{H}\right)+\delta\bar{A}\mathrm{rot}\bar{H}\tag{5}$$

and

$$\begin{aligned}&\nu\,\mathrm{div}\bar{A}\cdot\mathrm{div}\delta\bar{A}=\mathrm{div}\left(\delta\bar{A}\cdot\nu\,\mathrm{div}\bar{A}\right)-\\&-\delta\bar{A}\mathrm{grad}\left(\nu\,\mathrm{div}\bar{A}\right)\end{aligned}\tag{6}$$

are given by the general Gauss theorem and conservation of vector potential conservation A to the pass of discontinuity surface S. Variation δA is arbitrary chosen. Equation (5) imposes:

$$\mathrm{rot}\bar{H}-\bar{J}-\mathrm{grad}\left(\nu\,\mathrm{div}\bar{A}\right)=0\ \text{in D}\tag{7}$$

$$\nu\,\mathrm{div}\bar{A}=0\ \text{on}\ \Sigma\tag{8}$$

$$\bar{n}_S\times\left[\bar{H}\right]_S=\bar{J}_S\tag{9}$$

the passing condition on the discontinuity surface. Applying the divergence operator of the first equation (4) result:

$$\Delta\left(\nu\,\mathrm{div}\bar{A}\right)=0\tag{10}$$

Other two equations (8) and (10) demonstrate that the function νdivA is harmonic in the computing field D and null for its boundary. The first equation becomes one of the first law of steady state magnetic field validating as functional (1).

Under the hypothesis: fix, nonlinear, anisotropic, non-homogeneous and continuous magnetized substituting the following equation [6]:

$$\bar{H}\left(\bar{r}\right)=\bar{\bar{\nu}}\left(\bar{B},\bar{r}\right)\cdot\left[\bar{B}\left(\bar{r}\right)-\bar{B}_r\left(\bar{r}\right)\right],\tag{11}$$

where ν is magnetic reluctivity which is inverse of magnetic permeability μ, result the functional:

$$\begin{aligned}&\Im_4\left(\bar{A}\right)=\int_D\left\{\int_{\bar{0}}^{\bar{B}}\bar{\bar{\nu}}(\bar{B},\bar{r})(\bar{B}-\bar{B}_r)d\bar{B}-\bar{J}\bar{A}+\frac{1}{2}\left\|\nu\right\|_{\bar{B}=0}(\mathrm{div}\bar{A})^2\right\}dD+\\&+\int_\Sigma\left(\bar{H}x\bar{A}\right)\bar{n}_\Sigma d\Sigma-\int_s\bar{J}_s\bar{A}dS\end{aligned}\tag{12}$$

where $\left\|\nu\right\|$ is canonical form of square matrix associated to symmetrical two order tensor of reluctivity.

In case of computing fields with fix, linear, isotropic, homogeneous and without permanent magnetization bodies, reluctivity ν is a scalar constant, and $\bar{B}_r=0$. The specific form of functional is:

$$\Im_4\left(\bar{A}\right)=\int_D\left\{\frac{\nu}{2}\sum_{\lambda=1}^{3}\left|\mathrm{grad}A_\lambda\right|^2-\bar{J}\bar{A}\right\}dD-\int_{\Sigma_N}\nu\bar{A}\cdot\frac{\partial\bar{A}}{\partial n_{\Sigma_n}}d\Sigma_N\tag{13}$$

where sum refers to other three scalar components of vector magnetic potential $\bar{A}$.

Variation of functional given in [6] results from (13):

$$\begin{aligned}&\delta\Im_4\left(\delta\bar{A}\right)=\int_D\left\{\nu\sum_{k=1}^{3}\left(\mathrm{grad}\,A_k\cdot\mathrm{grad}\,\delta\cdot A_k-J_k\cdot\delta\cdot A_k\right)\right\}dD-\\&-\int_{\Sigma_n}\nu\sum_{k=1}^{3}\frac{\partial A_k}{\partial n_{\Sigma_N}}\delta A_k d\Sigma_n=\\&\int_D\left\{\sum_{k=1}^{3}\left(\nu\Delta A_k+J_k\right)\right\}dD-\int_{\Sigma_N}\nu\sum_{k=1}^{3}\left(\mathrm{grad}A_k\cdot\bar{n}_{\Sigma_N}-\frac{\partial A_k}{\partial n_{\Sigma_N}}\right)\delta A_k d\Sigma_N+\\&+\int_{\Sigma_D}\nu\sum_{k=1}^{3}\mathrm{grad}A_k\cdot\bar{n}_{\Sigma_N}\delta A_k d\Sigma_N=0\end{aligned}\tag{14}$$

In this equation, the following vectorial identity:

$$\mathrm{grad}A_k\cdot\mathrm{grad}\delta A_k=\mathrm{div}(\delta A_k\cdot\mathrm{grad}A_k)-\Delta A_k\delta A_k\tag{15}$$

as well as Gauss theorem were taken into account.

Equation (15) can be applied at arbitrary variations δA_k, k = 1, 2, 3 if:

$\Delta A_k = -\mu \bar{J}_k$, k = 1, 2, 3 in D, that means only Poisson equation of vector potential which takes into consideration the Coulomb standard calibration condition [6]:

$$grad A_k \cdot \bar{n}_{\Sigma_N} = \frac{\partial A_k}{\partial n_{\Sigma_N}} \quad \text{on } \Sigma_N \subset \Sigma, \tag{16}$$

which is an identity so that Neumann boundary condition:

$$\frac{\partial \bar{A}}{\partial n_{\Sigma_N}} = \bar{f}_N(\bar{r}), \bar{r} \in \Sigma_N \tag{17}$$

is a condition to natural limit;
δA_k=0, k=1,2,3 on Σ_D=Σ-Σ_N, this result as Dirichlet condition is an essential condition in (14).
In 3D problems in Cartesian coordinates (x,y,z), functional leads to the following equation:

$$\Im_4(\bar{A}) = \int_D \{\frac{v}{2} \sum_{\lambda=x,y,z} [(\frac{\partial A_\lambda}{\partial x})^2 + (\frac{\partial A_\lambda}{\partial y})^2 + (\frac{\partial A_\lambda}{\partial z})^2 - J_\lambda A_\lambda]\} dxdydz -$$
$$- \int_{\Sigma_N} v(\frac{\partial A_x}{\partial n_{\Sigma_N}} A_x + \frac{\partial A_y}{\partial n_{\Sigma_N}} A_y + \frac{\partial A_z}{\partial n_{\Sigma_N}} A_z) d\Sigma_N \tag{18}$$

2D bidimensional problems of steady state magnetic filed are by definition that problems in which the unknown term is a vector magnetic potential. This vector has the orientation of an axis of coordinate system and depends on other coordinates of the system.
2D problems in Cartesian coordinates (x,y,z) called plan-parallel as well as the current density have the orientation O_z and the vector magnetic potential has the structure $\bar{A}$ [0, 0, $A_z(x,y)$]. Therefore, functional reduces to:

$$\Im(A_z) = \int_D \{\frac{v}{2}[(\frac{\partial A_z}{\partial x})^2 + (\frac{\partial A_z}{\partial y})^2] - J_z A_z\} dxdy$$
$$- \int_{\Gamma_N} v g_N(x,y) A_z d\Gamma_N \tag{19}$$

where the computing field called D is a surface plane, and Γ_N plan boundary (form) which is narrowed its.
Numerical simulation is realized by using a finite element package ANSYS. This programme assumes three stages: preprocessor, solver and postprocessor. The procedure for doing a static magnetic analysis consists of following main steps: create the physics environment, build and mesh the model and assign physics attributes to each region within the model, apply boundary conditions and loads (excitation), obtain the solution, review the results.
In order to define the physics environment for an analysis, it is necessary to enter in the ANSYS preprocessor (PREP7) and to establish a mathematical simulation model of the physical problem [3].
In order to this the following steps are presented below: set GUI Preferences, define the analysis title, define element types and options, define element coordinate systems, set real constants and define a system of units, define material properties.
ANSYS includes a variety of elements which can be used in modeling the electromagnetic phenomenon [3]. Element types establish the physics of the problem domain. Depending on the nature of the problem, you may need to define several element types to model the different physics regions in the model.
In present application, for the modeling of the magnetostatic field we choose SOLID97 element, which permits three dimensional magnetic field modeling in planar and asymmetric problems (Fig.3).

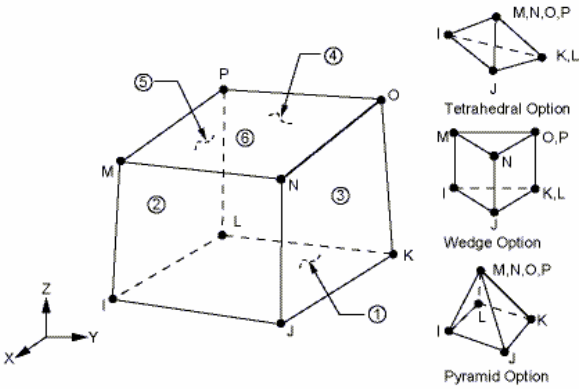

Fig.3 SOLID97 Element Description [3]

The element is defined by eight nodes, and has up to five degrees of freedom per node out of six defined DOFs; that is, the magnetic vector potential (AX, AY, AZ), the time-integrated electric potential (VOLT - classical formulation) or the electric potential (VOLT - solenoidal formulation), the electric current (CURR), and the electromotive force (EMF). SOLID97 is based on the magnetic vector potential formulation with the Coulomb gauge, and is applicable to the following low-

frequency magnetic field analyses: magnetostatics, eddy currents (AC time harmonic and transient analyses), voltage forced magnetic fields (static, AC time harmonic and transient analyses), and electromagnetic-circuit coupled fields (static, AC time harmonic and transient analyses). The element has nonlinear magnetic capability for modeling B-H curves or permanent magnet demagnetization curves [3].

After defining element types and options, if you have laminated materials aligned in an arbitrary manner you need to identify the element coordinate system or systems to be used. The Global Cartesian coordinate system is the default. You can specify a different coordinate system by specifying its origin location and orientation angles. The coordinate system types available are Cartesian, cylindrical (circular or elliptical), spherical (or spherical), and toroidal. Once it has defined one or more element coordinate systems, it can set a pointer that identifies the coordinate system to be assigned to subsequently defined elements (area and volume elements only).

The ANSYS material library contains definitions of several materials with magnetic properties. Instead of defining material properties from scratch, you can read these material properties into the ANSYS database and, if necessary, modify them to match the materials in your analysis problem more closely [3].

The copper property presents temperature-dependent resistivity and relative permeability. All other properties are B-H curves.

Also in this phase we choose and define the materials. For the path of current and the slopes copper has been chosen. For the two ferromagnetic plates, steel from ANSYS library has been chosen with the material properties contained in the emagM3.SI_MPL, emagM54.SI_MPL and emagVanad.SI_MPL files.

Materials with magnetic properties defined in the ANSYS material library are as follows Table 1.

Table 1. Materials with magnetic properties

Material	Material Property File Containing Its Definition
Copper	emagCopper.SI_MPL
M3 steel	emagM3.SI_MPL
M54 steel	emagM54.SI_MPL
SA1010 steel	emagSa1010.SI_MPL
Carpenter (silicon) steel	emagSilicon.SI_MPL
Iron cobalt vanadium steel	emagVanad.SI_MPL

The arcing chamber along with the path of current are put together in a box and inside of it air has been defined as material property.

ANSYS offers the possibility of constructing the geometric model as well as importing it from a CAD program [3].

Next step in preprocessor phase is mesh generation and load applying upon the elements. We used a mesh with 3335 nodes and 1606 triangular elements. The finite element mesh of the arcing chamber is shown in Fig.4.

.

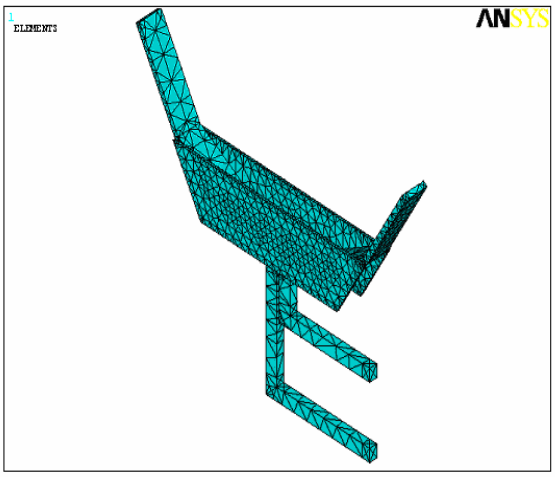

Fig.4 Meshing the model with triangular elements

You can apply boundary conditions and loads to a 2-D static magnetic analysis either on the solid model (key points, lines, and areas) or on the finite element model (nodes and elements). The ANSYS program automatically transfers loads applied to the solid model to the mesh during solution [3].

This specifies applied current to a source conductor. The units of J_S are amperes/meter^2 in the MKS system. For a 2-D analysis, only the Z component of J_S is valid; a positive value indicates current flowing in the +Z direction in the planar case and the -Z (loop) direction in the asymmetric case. Current density applies directly on the finite elements which form the conductors (the slope). The current density is given in SI units (A/m^2). The applied boundary conditions are Dirichlet condition, A=0.

Next, you define which solver you want to use. You can specify any of these values: Sparse solver (default), Frontal solver, Jacobi Conjugate Gradient (JCG) solver, JCG out-of-memory solver, Incomplete Cholesky Conjugate Gradient (ICCG) solver, Preconditioned Conjugate Gradient solver (PCG), PCG out-of-memory solver [3].

The solver takes a set of data files that describe problem and solves the relevant Maxwell's

equations to obtain values for the magnetic field through the solution domain [1].
The primary unknowns are nodal values of the magnetic vector potential and their derivatives are the secondary unknowns (flux density).

3 Results

This is a graphical program that displays the resulting fields in the form of contour and density plots. The program also allows the user to inspect the field at arbitrary points, as well as evaluate a number of different integrals and plot various quantities of interest along user-defined contours. The path for the displayed charts is chosen between two points placed symmetrical one from another on the trapezoidal ferromagnetic plate at a distance of 160 mm and 15 mm spaced from the current path.
It's also possible to save the plotted results in EMF format (Extended Metafile).

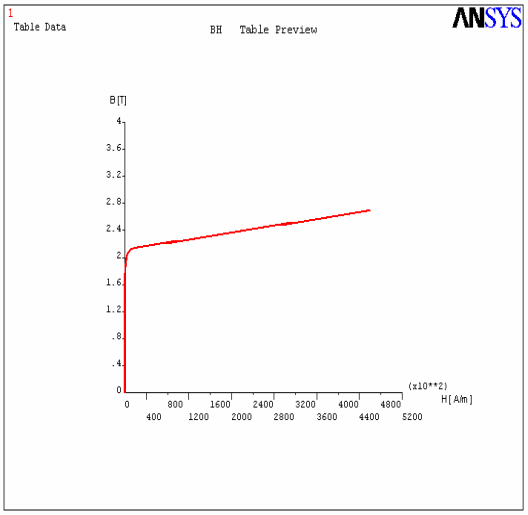

Fig.5 Magnetization curve of the emagM3

BH curve presents real dependency magnetic flux density on magnetic flux intensity in ferromagnetic materials. It is a non-linear dependency which means higher requests for calculation process. The nonlinear B-H curve of the ferromagnetic material used for the slopes is presented in Fig.5, Fig.7 and Fig.9.
Arcing chamber model along with current path are built-in together in a box, inside of which air has been defined as material property.
Magnetic flux density spectrum in ferromagnetic shapes is represented in Fig.6, Fig.8, and Fig. 10 for the three used ferromagnetic materials [7].

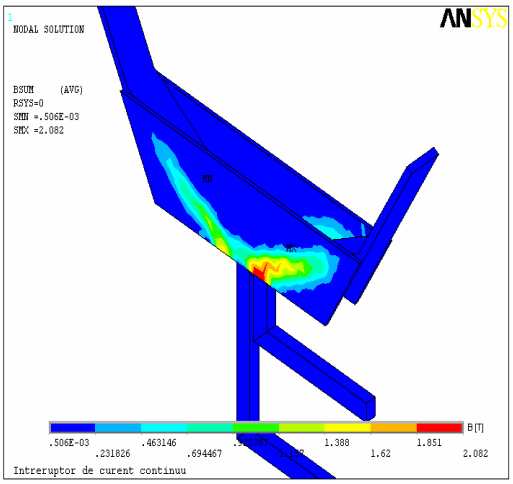

Fig.6 Distribution of magnetic flux density for EmagM3

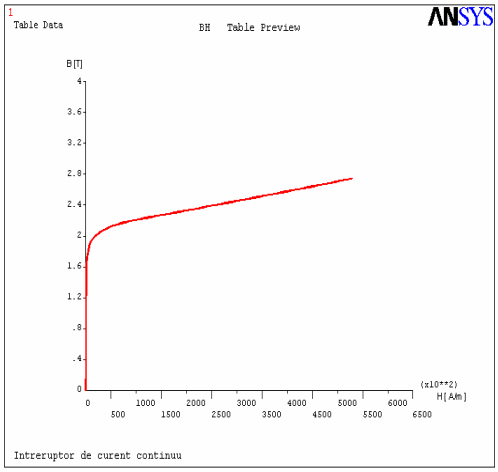

Fig.7 Magnetization curve of the emagM54

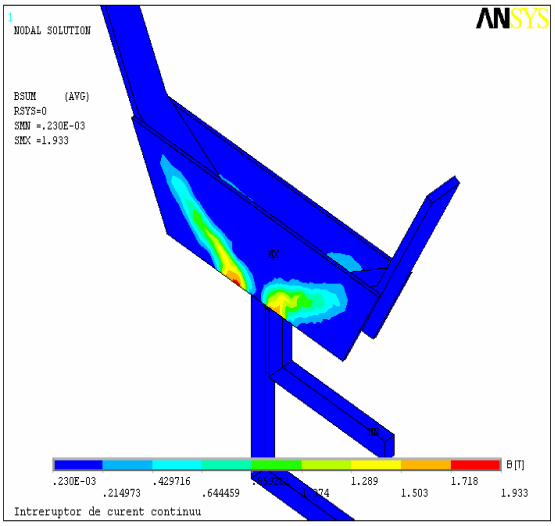

Fig.8 Distribution of magnetic flux density for EmagM54

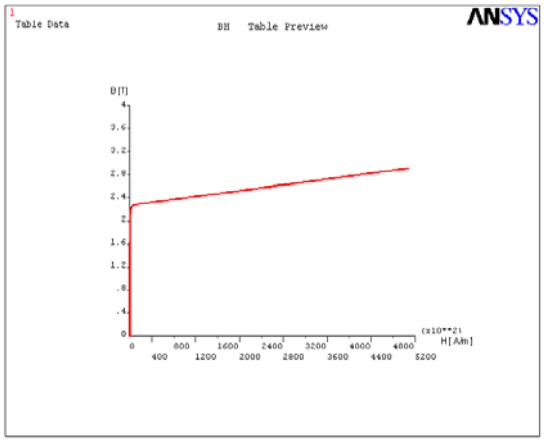

Fig.9 Magnetization curve of the emagVanad

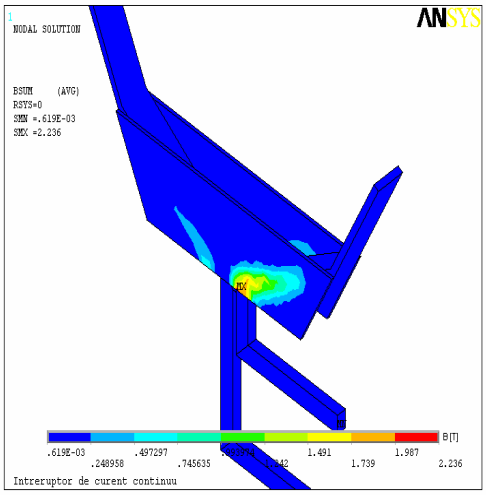

Fig.10 Distribution of magnetic flux density for Emag Vanad

In Fig.11 is shown variation of magnetic flux density depending on the ferromagnetic material type.
Thus, for EmagM3 steel is obtained a 2.082 [T] maximum value for the magnetic flux density; for EmagM54 steel maximum value is 1.933 [T] and for cobalt-vanadium steel EmagVanad the maximum value is 2.236 [T].

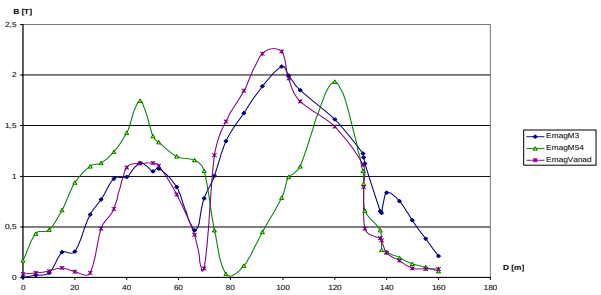

Fig.11 Variation of magnetic flux density depending on the ferromagnetic material type

Comparing the magnetic flux density spectrums in the three cases we can observe that maximum blow-out effect is obtained by using EmagVanad for the ferromagnetic shapes. For this material we obtain an optimal distribution for the magnetic field in the circuit breaker arcing chamber, which leads to a rapid movement of the electric arc towards the ferromagnetic plates. Arc quenching and arc voltage limiting occurs in base of the niche effect principle along with the electrode effect [7].

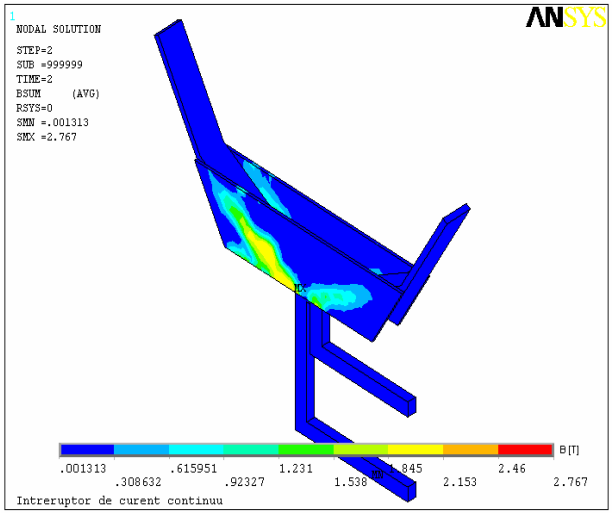

Fig.12 Distribution of magnetic flux density for the slope angle of 120^0

The distribution of magnetic flux density in the feromagnetic plates 7 and 9 is shown in Fig.12, Fig.13 and Fig.14 for the angle of slopes of 120^0, 110^0 and 130^0. Therefore, for the slope with an angle of 120^0 a maximum value is obtained for a magnetic flux density of 2.030 [T], for the slope with an angle of 110^0 a maximum value is obtained for a magnetic flux density of 1.275 [T] as well as the slope with an angle of 130^0 a maximum value is obtained for a magnetic flux density of 1.542 [T].
As it is observed from this analysis the magnetic blow-out effect is conditioned as the ferromagnetic material type used as well as the slope angle. The recommended optimum value for the slope angle is 120^0.
In Fig.15 is shown variation of magnetic flux density depending on the slope angle.
The current – limiting circuit breaker analyzed in this paper was designed and manufactured in Romania at Research and Development Institute for Electrical Engineering (ICPE) of Bucharest [11].

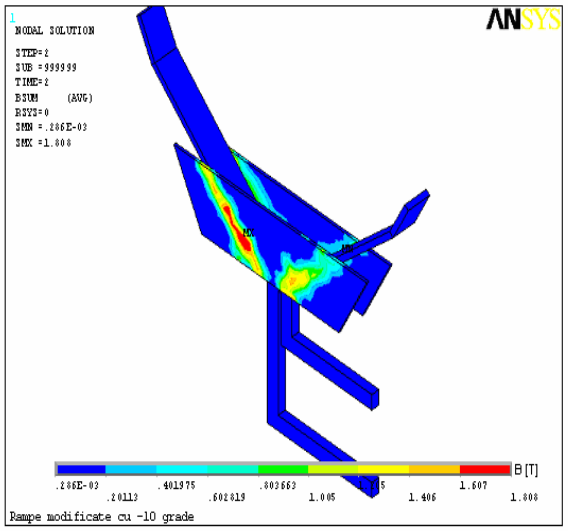

Fig.13 Distribution of magnetic flux density for the slope angle of 110^0

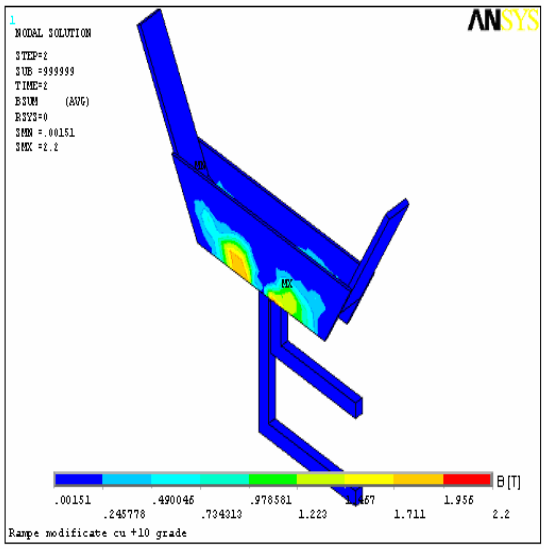

Fig.14 Distribution of magnetic flux density for the slope angle of 130^0

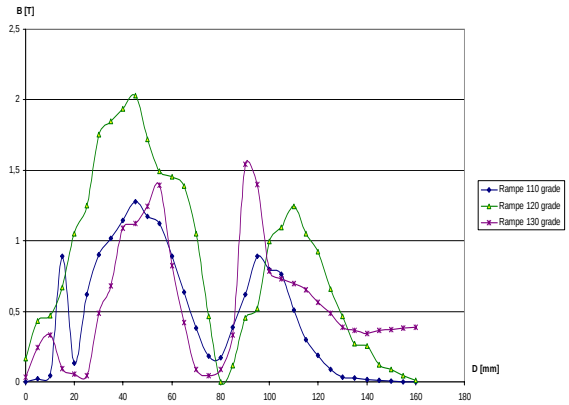

Fig.15 Variation of magnetic flux density depending on the slope angle.

Fig.16. Current – limiting circuit breaker [11]

4 Conclusions

The obtained results by simulation using ANSYS package confirms that this numerical computation of magnetostatic field in the current-limiting circuit breaker's arcing chamber leads to an accurate result.
It's well known that in electromechanical construction of a switching device, the arcing chamber along with current paths and contacts, represents the all-important elements concerning switching performances of these in normal operating conditions as well as in fault operating.
Using EmagVanad for ferromagnetic plates and value for the slope angle of 120^0 a maximum blow-out effect is obtained. Therefore, an optimal distribution of the magnetic field in the circuit breaker arcing chamber leads to a rapid movement of the electric arc towards the ferromagnetic plates.

References:

[1] Morozionkov, J., Virbalis, J.A., Investigation of Electric Reactor Magnetic Field using Finite Element Method, *Electronics and Electrical Enginnering*, No.5(85), 2008, pp. 9-12, ISSN 1392-1212;
[2] ABB circuit breakers for direct current application, Tehnical application papers, September 2007:
[3] ANSYS Guide Documentation;
[4] Hortopan G., Aparate electrice de comutație, Vol. II, Editura Tehnică, Bucharest, 1996;
[5] Garzon, R.D., High voltage circuit breakers-Design and Applications, Taylor and Francis Ed., 2002;

[6] Fireteanu, V. Numerical modelling of electromagnetic fields in electrotechnic devices, Master course notes, Politehnica *University of Bucharest,* 1998;
[7] Vîrjoghe, E.O., Truşcă, V., Optimizarea sistemului de suflaj al camerei de stingere pentru întreruptorul limitator de curent continuu - *E.E.A. Electrotehnica*, Vol.51, nr.2, apr-iun.2003, pp.6-9, ISBN: 1582-5175;
[8] Ionel, M., Stan, M.F., Sălişteanu I.C., Ionel, M.O. Advanced command techniques of electrical induction machines, *Proceedings of the 9th WSEAS International Conference on Power Systems (PS '09)*, Budapest, Hungary, September 3-5, 2009, pp.176-180, ISSN 1790-5117.
[9] MA Ai-qing, JIANG Xiu-chen, ZENG Yi, Research on the MPCG Algorithm applied in the three dimensional electric field calculation of SF_6 Circuit Breaker in three-phase-in-one tank GIS, WSEAS TRANSACTIONS on SYSTEMS, Issue 12, Volume 7, December 2008, pp.1392-1401, ISSN: 1109-2777;
[10] Zamanan, N., Sykulski, J.K., Modelling arcing high impedances faults in relation to the physical processes in the electric arc, WSEAS TRANSACTIONS on SYSTEMS, Issue 8, Volume 1, August 2006, pp.1507-1512, ISSN: 1790-5060;
[11] Research and Development Institute for Electrical Engineering (ICPE) of Bucharest, Romania, web site http://www.icpe.ro.